Published in final edited form as:
Comput Biol Med. 2011 June ; 41(6): 361–366. doi:10.1016/j.compbiomed.2011.03.014.

Investigating a compact phantom and setup for testing body sound transducers

Hansen A Mansy[a,b], **Joshua Grahe**[a], **Thomas J Royston**[b], and **Richard H Sandler**[a]

[a]Department of Pediatrics, Rush University, 1725 W Harrison Street, Suite 946, Chicago, IL 60612, USA

[b]Department of Mechanical and Industrial Engineering and Department of Bioengineering, University of Illinois at Chicago, 842 W Taylor Street, Rm 2039 ERF, Chicago, IL 60607

Abstract

Contact transducers are a key element in experiments involving body sounds. The characteristics of these devices are often not known with accuracy. There are no standardized calibration setups or procedures for testing these sensors. This study investigated the characteristics of a new computer-controlled sound source phantom for testing sensors. Results suggested that sensors with different sizes require special phantom requirements. The effectiveness of certain approaches on increasing the spatial and spectral uniformity of the phantom surface signal was studied. Non-uniformities >20 dB were removable, which can be particularly helpful in comparing the characteristics of different size sensors more accurately.

Keywords

Acoustic transducers; Stethoscope; Phantom; Sound source; Sensor testing; Vibration isolation; Spectral whitening

1. Introduction

Contact transducers are a key element in vibroacoustic experiments that require measuring body sounds. Previous studies used different transducers such as electronic stethoscopes and accelerometers that may vary in size, sensitivity, and frequency response [1]. Sensor characteristics are often not accurately known apriori and there is no standardized calibration setup or procedure for testing these sensors [2]. However, many attempts to compare the characteristics of the different sensors were carried out [3–10]. These comparisons can aid optimal sensor selection and facilitate evaluating the results from different studies that used different sensors.

Previous approaches of sensor testing used actual body sounds [3,4] or specially designed phantoms. The advantage of having a phantom is the ability to have a reproducible acoustic input for the sensors being tested [5]. Basic phantom designs included sound sources buried

Conflict of interest statement
None declared

in viscoelastic materials [6,7], water-filled polymer or latex bladders [8,9], electromagnetic speakers covered with viscoelastic layers [2], and a sound source coupled to the sensor with an air chamber [10]. While many earlier studies were successful in providing estimates of relative response of some sensors [2,3,5,6], the acoustic characteristics of most phantoms remain essentially undocumented. We believe that a better understanding of the phantom performance can help its optimal use for testing sensors. While there does not seem to be enough published sensor testing results from stethoscope manufacturers, this does not negate that internal tests are performed. In fact, the absence of published information highlights the need for standard test methods and more published information.

The objective of this study is to investigate the characteristics of a new phantom setup that can be used for testing transducers that have different sensitivity, frequency response, and contact area size. Desired phantom characteristics include elastic properties similar to soft tissue, temporal stability, compact size, ease of manufacturing, and high spatial and spectral uniformity of the acoustic energy at the phantom surface.

2. Methods

2.1 Phantom building Materials

There are two essential phantom components: a sound source and a coupling material that comes in direct contact with the sensor surface and mimics the properties of biological soft tissue. Sound sources used in earlier studies included electromagnetic speakers [2,6] and shakers [11], which can be relatively large and/or heavy. To minimize the phantom weight and volume, a light weight (3 gm, 5 cm diameter, and 0.3 cm thick) piezo-electric speaker (VSB50EWH0301B, muRata, Rockmart, GA) was chosen as the sound source. Coupling materials used in previous studies included gelatin [7,12], different elastomers [2,6], water bladders [9], and air columns [10]. While many studies [13] documented gelatin mechanical properties, relevant properties of candidate elastomers were not investigated until recently [14]. The latter study elucidated the challenges in testing these elastomers and documented some of their mechanical properties relevant to constructing tissue mimicking phantoms. More specifically, the study measured the modulus of elasticity under dynamic loading conditions, the mass density, and the stability of material properties for 9 different elastomers over extended periods of time. Based on these results, a highly stable, easy to handle, and low cost elastomer (Semicosil 921, Wacker Solutions, Adreian, MI) was chosen for building the current phantom.

2.2 Phantom dimensions, design, and construction

The overall phantom size was chosen to accommodate the largest contact sensor used in this study, which was an electronic stethoscope that has a contact area diameter of 4 cm. Such size is typical of electronic stethoscopes. The phantom diameter was, therefore, chosen as 10 cm to be significantly larger than that sensor. A schematic of phantom assembly is shown in Figure 1. Here, the piezoelectric speaker is buried (1.5 cm) below the phantom surface. The speaker element top is in direct contact with the elastomer to maximize vibro-acoustic energy coupling to the phantom surface. The element bottom surface was separated from the elastomer by an air gap (0.5 cm deep) to reduce acoustic loading and coupling at the lower surface, which can help direct more of the speaker acoustic energy upward towards the phantom surface.

To construct this phantom, the elastomer was cast into two steps. In the first step, a 2.5 cm deep layer of elastomer was poured into a thin cylindrical plastic container with 10 cm diameter. To reserve space for the speaker in this layer, a solid cylindrical plastic rod (5 cm diameter) was held coaxially while the elastomer cured. The rod was sprayed with a special

coating (Ease-Release, Smooth-On, Easton, PA) to facilitate its removal from the cured elastomer. This created a cylindrical space (5 cm diameter and 0.8 cm deep) in that elastomer layer to accommodate the speaker assembly.

The speaker (Sec 2.1) was made of a metal disc attached to a plastic rim with the latter having inner and outer diameters of 4 and 5 cm, respectively, and thickness of 0.3 cm. To create an air gap below the disc, a plastic ring (4 and 5 cm inner and outer diameters and 0.5 cm high) was glued to the rim. This speaker assembly (5 cm outer diameter, 0.8 cm thickness) was then placed in the space created in the first elastomer layer. The speaker wires exited the phantom from its side wall via a small (1.5 mm diameter) hole in the container. In the final step, the second elastomer layer (1.5 cm deep and 10 cm diameter) was then poured after speaker placement.

The results of testing the phantom suggested building a second design where a metal plate (0.2 cm thick, 8 cm diameter) was added between the speaker and phantom surface (see Figure 2). This modified design was constructed by casting three elastomer layers (instead of two for the original design). The first layer was identical to that of the original design including the speaker assembly. The second layer (0.3 cm deep and 10 cm diameter) was cast after the first layer cured and the speaker assembly was in place. The metal plate was then placed over the cured second layer and covered by casting the final elastomer layer (1 cm thick).

2.3 Phantom testing

To measure the acoustic signal at the phantom surface a laser Doppler vibrometer (LDV) (LSV 6000, Polytec, Tustin, CA) was placed 50 cm from the surface with the laser beam directed perpendicular to the surface. The device has an accurate calibration and performs a non-contact (hence no surface loading) surface velocity measurement in the direction perpendicular to the surface. Measurement points were arranged along 2 perpendicular axes of symmetry intersecting at the center of the phantom surface. The spacing between the points was 1 cm with one point placed at the surface center. Small square pieces (0.15 cm diameter) of retroreflective tape were placed at the measurement points to provide sufficient laser reflection that ensures reliable vibrometer operation.

2.4 Input signal generation

The speaker inside the phantom was driven by a power amplifier (40W, Radioshack, Fort worth, TX). A computer (Inspiron, 9200, Dell, Round Rock, TX) provided the amplifier with an input signal using commercial software (ver 7.4, Matlab, The Maththworks Inc., Naitck, MA) and a data acquisition card (DAQCard-6062E, National Instruments, Austin, TX). The phantom input signal was a band-limited white noise that was generated from a random number generator and then filtered using a band-pass digital filter (8^{th} order Butterworth, 100–2000 Hz pass-band). This signal was further manipulated (Sec 3.2) to provide uniform vibration spectra at the phantom surface.

2.5 Isolation from ambient noise

Previous studies have attempted to isolate the phantom by conducting studies in sound proof rooms and by placing phantoms on foam. In the current study, the phantom and vibrometer were also placed in a sound proof room (MDL 4230S, Whisper Room, Morristown, TN). To reduce the effect of floor vibrations on the phantom, the phantom was placed on a platform suspended by four identical springs. The platform mass and the spring constants were chosen to provide a natural frequency around 2 Hz. Hence, the platform-spring assembly behaved as a second order (mass-spring) mechanical system that inhibits frequencies greater than 2 Hz from reaching the phantom at a rate of −40 dB/decade. For example, a 20 Hz and

200 Hz floor vibrations would be inhibited at the platform surface by about 40 and 80 dB, respectively. To measure the effectiveness of this setup in inhibiting floor vibrations an accelerometer (333B50, 1V/g, PCB Piezotronics, Depew, NY) was used to measure the vibration levels at the platform and floor while a white noise source was placed on the floor.

2.6 Sensor testing set up

Figure 3 shows the setup used to quantify sensor response to desired input signals (played through the phantom) and to ambient noise. Here the phantom receives a computer-generated signal and produces a desired acoustic signal at its surface. The amplitude of the surface signal was adjusted to be similar to the typical body sound amplitude (such as normal tracheal sounds). This was achieved by matching the stethoscope output amplitude in response to phantom surface signal to that of normal tracheal breath sounds. An electromagnetic "ambient noise speaker" (Model 40–1432, RadioShack, Fortworth, TX) was placed 50 cm from the phantom surface to introduce simulated room ambient noise (Band-limited white noise 100–2000Hz) with an amplitude of 75 dB SPL measured in air at the model surface using a sound level meter (Model 33–2055, RadioShack, Fortworth, TX). The computer and data acquisition card (described above) also controlled data acquisition. Each acquisition lasted 15 seconds at a sampling frequency of 8192 Hz.

2.7 Sensor testing procedure

To test each sensor, each was placed directly over the phantom center. The sensor background noise, s_b, was estimated by measuring the sensor output while the phantom speaker and environment speaker were silent. The input to the phantom was then initiated and the sensor output, s_{tb}, was recorded. This was followed by turning the phantom signal off and the ambient noise speaker on and acquiring the sensor output, s_{ab}. A similar procedure has been described in earlier studies [6,15]. The power spectra of all signals were estimated using an FFT based algorithm (implemented in Matlab, ver 7.4, The Mathworks Inc., Natick, MA). The spectra corresponding to s_b, s_{tb}, and s_{ab} were converted to a dB scale and named S_b, S_{tb}, and S_{ab}, respectively. The frequency-dependent signal-to-noise ratio (SNR) of each sensor (in dB) was estimated as (S_{tb} -S_b). The sensitivity to ambient noise was assessed by calculating (S_{ab} -S_b). The sensor sensitivity to tissue borne relative to airborne sounds was calculated as (S_{tb}- S_{ab}). Similar approaches were used previously [6,15] to estimate sensor sensitivity to tissue-borne and air-borne signals. An average value for each parameter was calculated in the 100–1000 Hz range.

3. Results and discussion

3.1 Floor vibration isolation

The transfer function between the vibration signals measured at the floor and at platform was calculated and is shown in figure 4. A transfer function drop at higher frequencies (e.g., f> 2 Hz) can be seen. The roll-off is about −40 dB/decade as theoretically expected for a 2nd order system [16]. This data suggests that the system can inhibit frequencies in the frequency range of interest (>100Hz) by at least 60 dB. Note that the range of frequencies considered here would cover most body sounds such as breath and gastrointestinal sounds. Heart sounds, however, have significant energy below 100Hz and hence, the frequency range would need to be expanded if heart sounds are to be considered.

3.2 Acoustic energy at the phantom surface

To investigate the characteristics of the phantom surface vibrations, the phantom was first placed on the vibration isolation platform. The phantom speaker was then excited by band-limited white noise (100 Hz <f<2000 Hz) and surface vibration signal was measured using

the LDV (Sec 2.3). Measurements were performed along 2 perpendicular axes of symmetry of the phantom surface. The typical differences between the vibration distribution along the two axes were small (< ±2dB). The average along the two perpendicular axes was calculated and normalized by dividing by the vibration amplitude at the surface center. Figure 5 shows the mean vibration distribution for both phantom designs (shown in Figure 1 and 2). It can be seen that the first design (without a metal plate), had a less uniform surface distribution where the acoustic energy decayed as we moved away from the phantom center. Hence, a sensor with a smaller area would, in the average, receive a louder signal than a sensor that has a larger contact area merely because of contact area differences. This can be a major drawback of any phantom that is used to compare sensors with different contact areas. This limitation may have existed in previous studies [2,6,9]. Some previous studies that measured surface vibrations in soft tissue models with subsurface excitation also reported uneven surface distributions [11,17].

The modified design of figure 2 attempted to solve this problem by adding a “uniformizing element” made of a sufficiently rigid plate that tends to move as one unit. The spatial distribution of the acoustic signal (Figure 5) shows that for the new design, symmetry has improved and a spatial non-uniformity of up to 20 dB was removed. Consequently, the diameter of the surface region with uniform signal (±1 dB) increased from about 1cm in the original design to 6 cm in the new design. This area is sufficiently large given that the maximum diameter of the sensors of interest was 4 cm in the current study. Since the area of uniformity (6 cm diameter) significantly exceeds the required area (4 cm diameter), the phantom can be made smaller (by using a smaller container and metal plate) while meeting the area uniformity requirement. For example, the phantom diameter may be decreased by 1–2 cm while keeping area of acoustic uniformity to ~ 4 cm in diameter. This can reduce phantom volume and mass by 20–40 %.

The spectrum of the signal at the phantom surface was also non-uniform (Figure 6). This is not surprising because the phantom transfer function is expected to be frequency dependent [2,11,15]. A non-uniform spectral distribution is not advantageous when trying to reliably estimate the frequency-dependent SNR of sensors. For example, at frequencies with high and low energy (at the phantom surface), the SNR may be over- and under-estimated, respectively. Hence, whitening of the surface signal would be desirable. Whitening was performed using hardware in a recent study [15]. In the current study, a software whitening approach was implemented to reduce the hardware requirements and keep the setup more compact. Here, the phantom input was filtered using information from the estimated phantom transfer function by implementing the following scheme:

1. Input a computer-generated band-limited white noise (100–2000 Hz) into the phantom.
2. Measure output at phantom surface and estimate the phantom transfer function.
3. Smooth the transfer function using a moving average filter.
4. Calculate the FFT of the original phantom input.
5. Divide the complex FFT coefficients by the smoothed transfer function.
6. Calculate the inverse FFT, store this signal, and use it as the new phantom input.

The resulting spectral distribution at the phantom surface is also shown in Figure 6, which shows that spectral non-uniformities of more than 25 dB were removed. The remaining spectral variations are less than ±1 dB in the 100–2000 Hz.

3.3 Senor testing

To validate the phantom usefulness for testing sensors with different footprints, two sensors were tested: the laser vibrometer (LSV 6000, Polytec, Tustin, CA) and an electronic stethoscope (Pishon, Seol, Korea). Figure 7 and 8 show the output spectra and coherence data for both sensors. The four lines in each figure show the sensor output spectra under four different conditions:

1. Only the phantom speaker is on (solid line), i.e., surface signal is present and the room speaker is silent. This signal estimates sensor sensitivity to tissue-borne sounds, S_{tb}.
2. Both phantom speaker and room speaker are on (dash-dot line), i.e., surface signal is present and the room speaker is on. This signal shows the combined response to the desired tissue borne signal and room airborne 75 dB noise (measured at the phantom surface).
3. Only the room speaker is on (dashed line), i.e. phantom speaker is silent and room airborne noise is 75 dB at the phantom surface. This signal estimates sensor sensitivity to room noise, S_{ab}.
4. No input signals to the phantom or room speaker (dotted line), i.e., phantom and room speakers are both silent. This provides an estimate of background noise, S_b.

When examining the first two conditions of Figure 7(a), it can be seen that the second condition (where the desired tissue borne signal and room noise co-exist), has an additional peak at 145 Hz, which lines up with the peak seen when the 75 dB room noise existed alone. The coherence data of Figure 7 (b) show that for the first condition (phantom speaker is activated while room noise is absent) the coherence is close to 100% as expected. However, when a 75 dB room noise co-existed, there was a coherence drop at 145 Hz suggesting that there is significant room noise contribution at that frequency. When the input signal was not sent to the phantom (the bottom 2 curves in the graph), coherence was close to zero as expected. Figure 8 (a) and (b) show the stethoscope response and coherence information. The data of Figure 8(a) suggest that there was little contribution of the room noise to the stethoscope signal when both tissue borne and room noise signals co-existed. Consequently, the drop in coherence due to the presence of room noise was minor as seen in Figure 8 (b).

It is worth noting that airborne sounds can “leak” into sensor output via two possible routes [6]. The first route is direct where the sensing element in the transducer is directly excited by the acoustic waves, while the second is indirect where acoustic signals excite soft tissue vibrations that are, in turn, detected by the sensor. Because of their design, air-coupled microphones are expected to be more susceptible to direct excitation than other types of contact sensors. The LDV, on the other hand, measures the phantom surface movement and ignores direct airborne signals. Hence, its output in the presence of airborne sounds (and silence of phantom speaker) provides a reasonable estimate of phantom surface vibrations due to airborne sounds.

The signal-to-noise-ratio for tissue borne and airborne signals were calculated as S_{tb}-S_b and S_{ab}-S_b respectively (Sec. 2.7). These ratios were 41.4 dB and 24.3 dB for the stethoscope, and 28.9 dB and 11.1dB for the LDV, respectively. The sensitivity of LDV to airborne noise suggests that airborne noise caused measurable surface movement. One possible method to reduce the contribution of airborne signals to tissue surface movement is to use bioacoustic insulators that surround transducers. Some success of this approach was reported [15] and found dependent on the sensor type. The sensor sensitivity to tissue borne sounds relative to that of airborne sounds can be calculated as the difference (S_{tb}-S_{ab}). This relative sensitivity was 17.8 dB for the LDV and 17.1dB for the stethoscope. The difference between the two

values is small, suggesting that the stethoscope (which has an air coupled microphone design) has appropriate insulation from airborne sounds in the current setup. While the current study focused on the effect of room noise on sensors during bench tests, future studies will investigate this effect in humans. Studying noise effects in human subjects is important for clinical applications and was addressed in some earlier studies [18,19].

4. Summary

Contact transducers are a key element in experiments involving body sounds. The characteristics of these devices are often not known with accuracy. Previous body sound studies used different sensor types and sizes. There are no established standardized calibration setups or procedures for testing these sensors. Further, the requirements for testing sensors with different sizes have not been studied in detail. Important requirements of the phantom, however, include elastic properties similar to soft tissue, temporal stability, compact size, and ease of manufacture. In addition, high spatial and spectral uniformity of the acoustic energy at the phantom surface are needed to accurately compare the characteristics of sensors with different contact area sizes.

The objective of the study was to investigate the performance of a computer-controlled phantom that can be used to test body sound sensors. The spatial distribution of acoustic output at the phantom surface was documented using a laser Doppler vibrometer. Significant spatial and spectral non-uniformities (> 25 dB) were detected. To improve spectral and spatial uniformity, a software scheme for spectral whitening was implemented and a rigid plate was embedded within the phantom.

The redesigned phantom demonstrated a high spatial and spectral uniformity (about ±1dB over a diameter > 4 cm and 100<f<2000 Hz) at its surface. Uniform signal distribution is particularly important for accurate comparison of the response of sensors with different contact areas. While the phantom was relatively compact, its size may be made smaller since its area with uniform acoustic amplitude exceeded the required area. The frequency range of operation was chosen to be 100–1500 Hz to cover most of the range of interest of many body sounds (such as breath and gastrointestinal sounds) [1, 20]. This frequency range may be easily expanded, if needed, by broadening the frequency band of the computer-generated phantom input.

The phantom also met other desired characteristics. For example, the elastomer used for building it has density and elasticity similar to soft tissue and high temporal stability. It is readily available, inexpensive, and easy to mold into desired shapes. The resulting phantom is compact (< 0.25 kg & < 0.25 liter), easy to build, and does not need any special storage or handling requirements.

The phantom was integrated in a setup that can evaluate sensor sensitivity to body sounds and environmental noise. The setup included an airborne sound generator and a compact floor vibration isolation component that significantly reduced (> 60 dB, f >100Hz) floor vibration transmission to the phantom. The setup was then placed in a sound proof room.

Initial tests of a few sensors suggest utility of the phantom and setup for testing sensors with different contact area sizes. The sensors included an electronic stethoscope and the laser vibrometer. The stethoscope (which contained an air-coupled microphone) was slightly more sensitive to airborne sounds, suggesting that it may have sufficient shrouding against airborne noise. Evaluation of sensors using a stable and consistent setup can help optimal choice of sensors as well as help compare measurements performed with different sensors.

Acknowledgments

This study was supported by the National Institutes of Health (NIH/NIDDK) grant number *R44 DK59685*. The authors would like to thank Dr. Bulent Ozer for his help with the laser Doppler vibrometer experimental setup and Mr. Daniel Elke for editing the manuscript.

References

1. Pasterkamp H, Kraman SS, Wodicka GR. Respiratory sounds. Advances beyond the stethoscope. Amer. J. Respir. Crit. Care Med. 1997 Sep..vol. 156:974–987. [PubMed: 9310022]
2. Kraman SS, Pressler GA, Pasterkamp H, Wodicka GR. Design, construction, and evaluation of a bioacoustic transducer testing (BATT) system for respiratory sounds. IEEE Trans. Biomed. Eng. 2006 Aug.; vol. 53(no. 8):1711–1715. [PubMed: 16916109]
3. Pasterkamp H, Kraman SS, DeFrain PD, Wodicka GR. Measurement of respiratory acoustical signals - Comparison of sensors. Chest. 1993 Nov..vol. 104:1518–1525. [PubMed: 8222817]
4. Kraman SS, Wodicka GR, Oh Y, Pasterkamp H. Measurement of respiratory acoustic signals. Effect of microphone air cavity width, shape, and venting. Chest. 1995 Oct..vol. 108:1004–1008. [PubMed: 7555110]
5. Kraman SS, Wodicka GR, Pressler GA, Pasterkamp H. Comparison of lung sound transducers using a bioacoustic transducer testing system. J. Appl. Physiol. 2006 Aug..vol. 101:469–476. [PubMed: 16627681]
6. Mansy, H.; Sandler, R.; Royston, T.; Jones, D. Testing sensors for body surface vibration measurements. 21st Annual International Conference of the Engineering in Medicine and Biology Society; Oct. 1999; Atlanta, GA, USA.
7. Royston TJ, Zhang X, Mansy HA, Sandler RH. Modeling sound transmission through the pulmonary system and chest with application to diagnosis of a collapsed lung. J Acoust. Soc. Am. 2002 Apr..vol. 111:1931–1946. [PubMed: 12002875]
8. Wodicka GR, Kraman SS, Zenk GM, Pasterkamp H. Measurement of respiratory acoustic signals. Effect of microphone air cavity depth. Chest. 1994 Oct..vol. 106:1140–1144. [PubMed: 7924486]
9. Watrous RL, Grove DM, Bowen DL. Methods and results in characterizing electronic stethoscopes. Comput. in cardio. 2002 Sept..vol. 29:653–656.
10. Abella M, Formolo J, Penney DG. Comparison of the acoustic properties of six popular stethoscopes. J. Acoust. Soc. Am. 1992; vol. 91:2224–2228. [PubMed: 1597610]
11. Royston TJ, Yazicioglu Y, Loth F. Surface response of a viscoelastic medium to subsurface acoustic sources with application to medical diagnosis. J. Acoust. Soc. Am. 2003 Feb..vol. 113:1109–1121. [PubMed: 12597204]
12. Royston TJ, Mansy HA, Sandler RH. Excitation and propagation of surface waves on a viscoelastic half-space with application to medical diagnosis. J. Acoust. Soc. Am. 1999 Dec..vol. 106:3678–3686. [PubMed: 10615706]
13. Hall TJ, Bilgen M, Insana MF, T, Krouskop A. Phantom materials for elstography. IEEE Trans. Ultrason. Ferroelectr. Freq. Control. 1997 Nov..vol. 44:1355–1365.
14. Mansy HA, Grahe JR, R, Sandler H. Elastic properties of synthetic materials for soft tissue modeling. Phys. Med. Biol. 2008 Apr..vol. 53:2115–2130. [PubMed: 18369277]
15. Zanartu M, Ho JC, Kraman SS, Pasterkamp H, Huber JE, Wodicka GR. Air-borne and tissue-borne sensitivities of bioacoustic sensors used on the skin surface. IEEE Trans. Biomed. Eng. 2009 Feb..vol. 56(no. 2) 443-4515.
16. Figliola RS, Beasley DE. Theory and Design for Mechanical Measurements. John Wiley & Sons Inc. 2006
17. Yazicioglu Y, Royston TJ, Spohnholtz T, Martin B, Loth F, Bassiouny HS. Acoustic radiation from a fluid-filled, subsurface vascular tube with internal turbulent flow due to a constriction. J. Acoust. Soc. Am. 2005 Aug..vol. 118:1193–1209. [PubMed: 16158674]
18. Pasterkamp H, Wodicka GR, Kraman SS. Effect of ambient respiratory noise on the measurement of lung sounds. Med. Biol. Eng. Comput. 1999 Jul..vol. 37:461–465. [PubMed: 10696703]

19. Groom D. The effect of background noise on cardiac auscultation. Am. Heart J. 1956; vol. 52:781–790. [PubMed: 13362080]

20. Mansy HA, Sandler RH. Detection and analysis of gastrointestinal sounds in normal and small bowel obstructed rats. Med. Biol. Eng. Comput. 2000 Jan..vol. 38:42–48. [PubMed: 10829389]

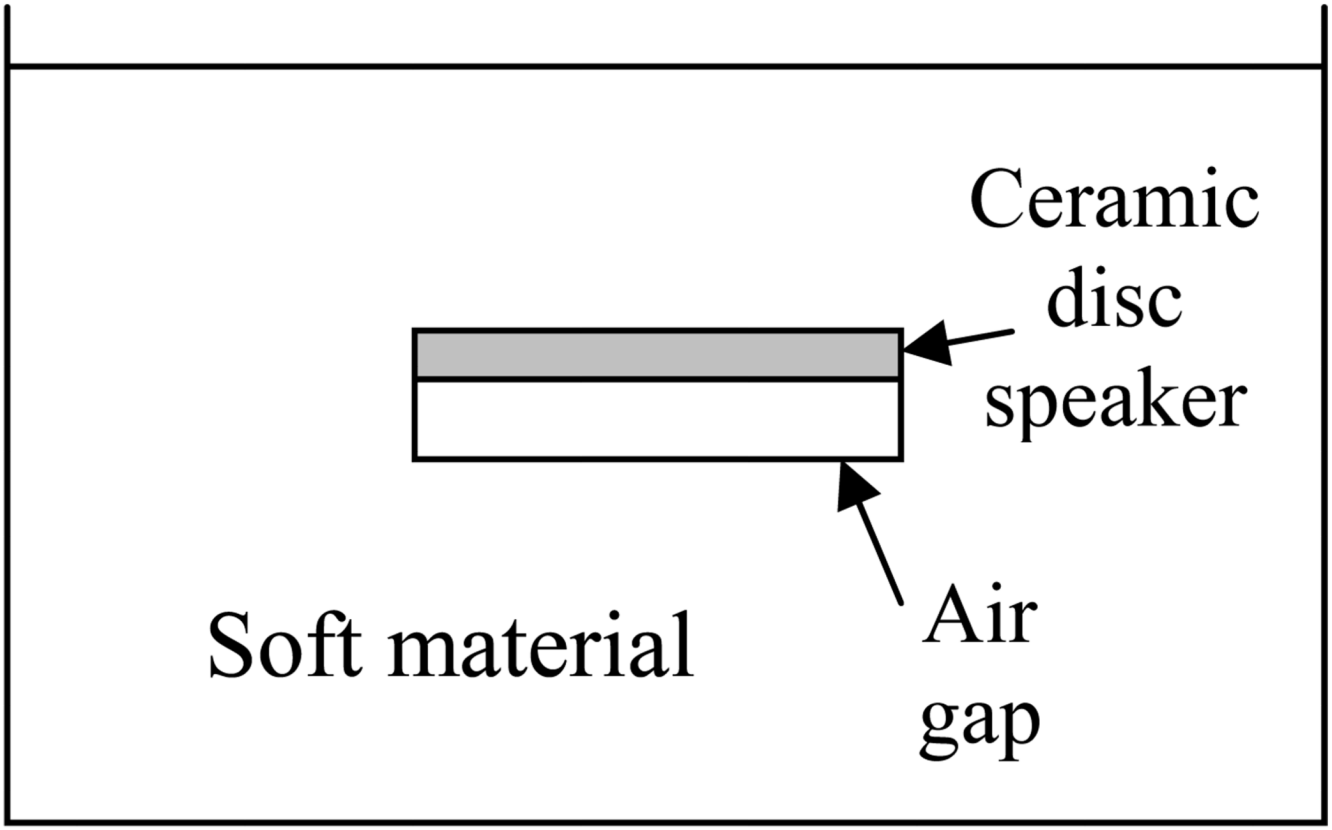

Fig. 1.
The initial design of the phantom that was used to test sensors. The sound source (ceramic piezoelectric disc) is buried in a material with elastic properties similar to living soft tissue. An air gap is placed below the sound source to create an acoustic impedance mismatch, which helps most of the acoustic output of the ceramic disc to go upward. This reduces loading and power input to the ceramic disc.

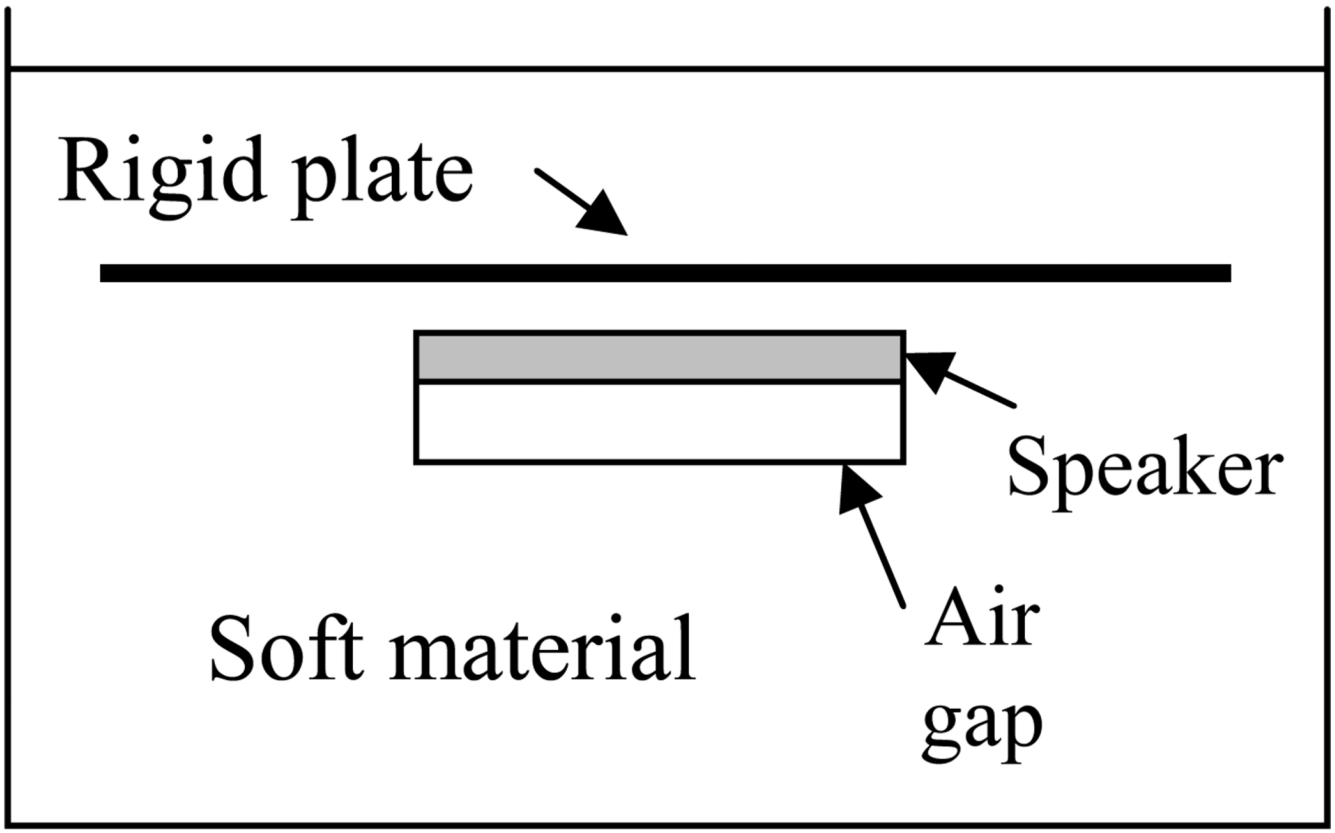

Fig. 2.

The final design of the phantom. The sound source (ceramic piezoelectric disc) is buried in a material with elastic properties similar to living soft tissue. A rigid plate is added between the sound source and phantom surface to help uniform ize the acoustic signal at the surface. A computer is used to tailor the spectra of the sound input to the ceramic disc so that the acoustic energy is equally distributed over the frequency range of testing.

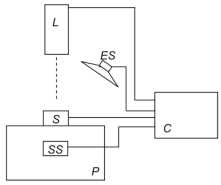

Fig. 3.

The sensor testing setup. C=Computer with a data acquisition card. ES=Speaker that inputs simulated environment noise around the setup, L=Laser vibrometer to measure signal at the phantom surface before testing each sensor, P=Phantom made of a material with soft tissue properties, S=Sensor to be tested, SS= Speaker implanted in the phantom to input the test signal that is to be measured by the sensor. The set-up is placed inside a sound-proof room.

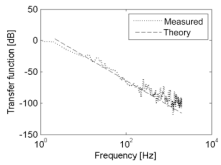

Fig. 4.

The transfer function of the floor vibration isolation platform.

A drop in the vibration of > 60 dB was possible in a broad frequency range (f > 100Hz). The dashed line shows the theoretical roll-off (−40dB/decade) of the corresponding spring-mass system.

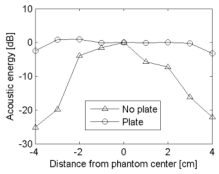

Fig. 5.

The acoustic energy distribution with and without a sufficiently rigid metal plate buried under the phantom surface. The plate was added to help uniformize the energy distribution. This is important because sensors of different diameters were to be tested. If the distribution is not uniform, sensors with different areas will receive a different input, which will introduce errors in comparing sensor outputs. It can be seen that the new phantom design (with the rigid plate) reduced acoustic energy non-uniformity by > 20 dB.

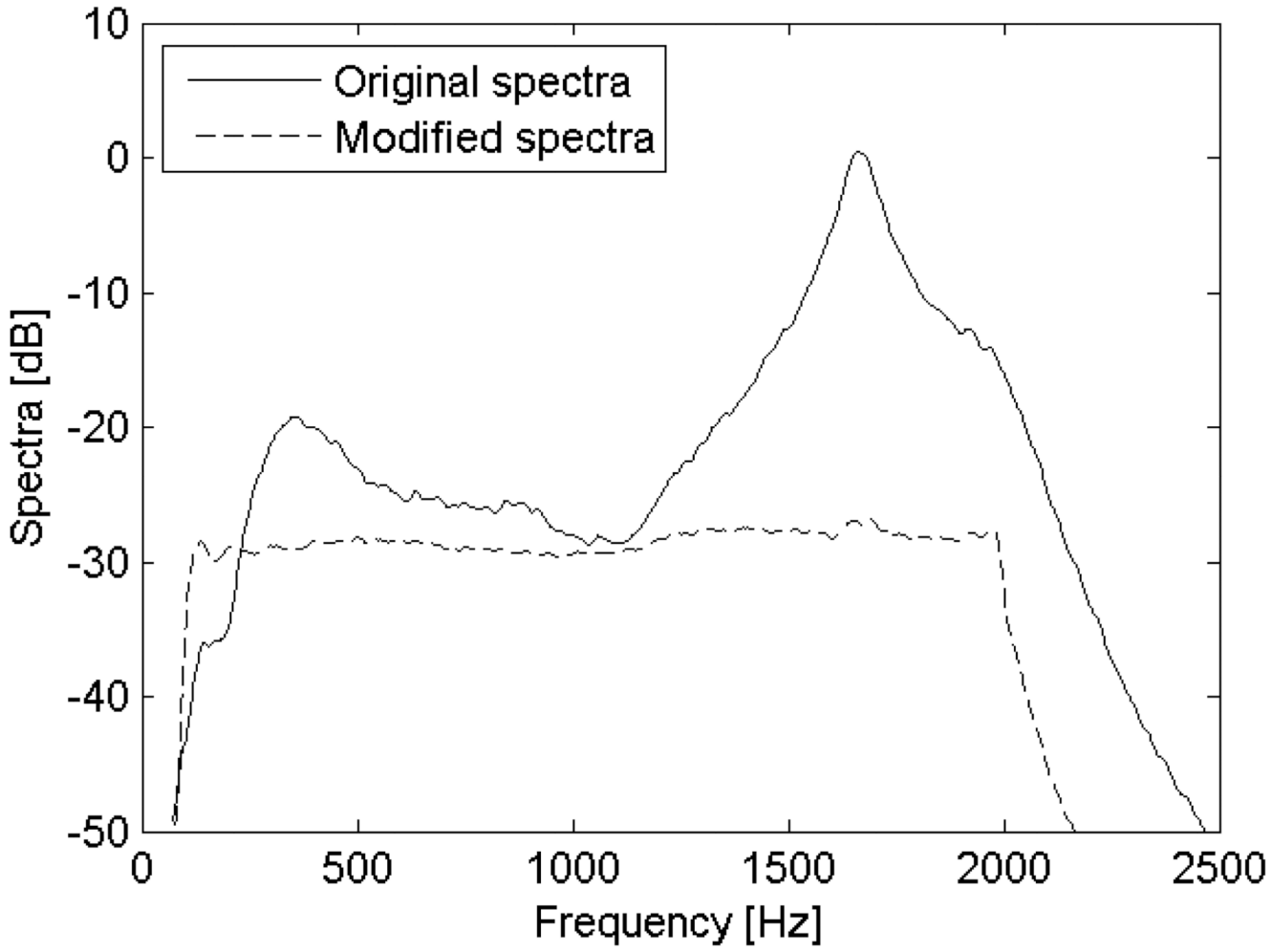

Fig. 6.

The spectra at the surface of the phantom before (solid line) and after (dashed line) spectral whitening of phantom output. Here, the computer calculated the “transfer function” of the phantom and redistributed the energy such that the phantom surface had a more uniform acoustic spectra. The data showed that non-uniformities of > 25dB were removable.

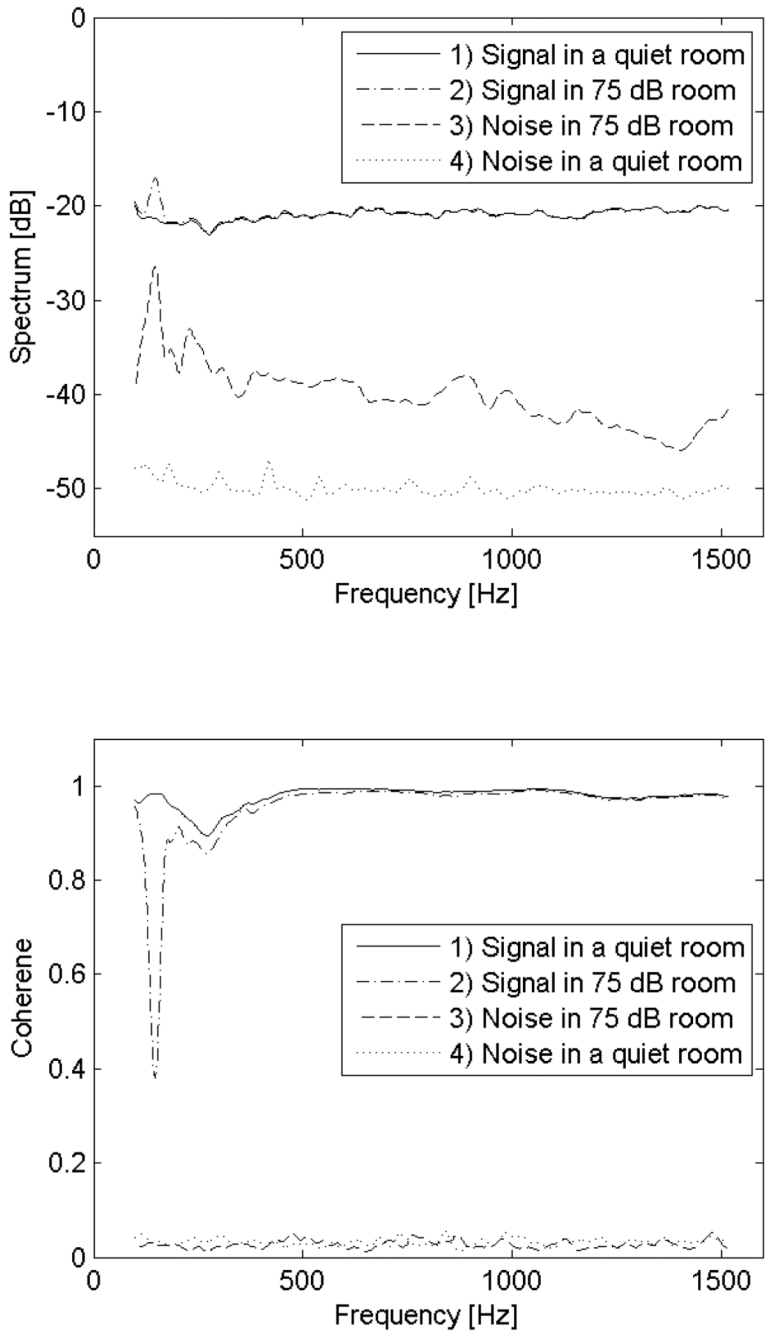

Fig. 7.

(a) The laser Doppler vibrometer output at different frequencies under four conditions: 1) in a quiet room while inputting a signal into the phantom (to measure contribution of the signal to the vibrometer output), 2) in a room with 75 dB noise while inputting a signal into the phantom, 3) in a room with 75 dB noise with no phantom input (to estimate room noise contribution to the vibrometer output), and 4) in a quiet room without a phantom input signal (to estimate the background noise)

(b) The coherence between laser Doppler vibrometer output and phantom input at different frequencies under four conditions: 1) in a quiet room while inputting a signal into the phantom, 2) in a room with 75 dB noise while inputting a signal into the phantom, 3) in a

room with 75 dB noise with no phantom input, and 4) in a quiet room without a phantom input signal.

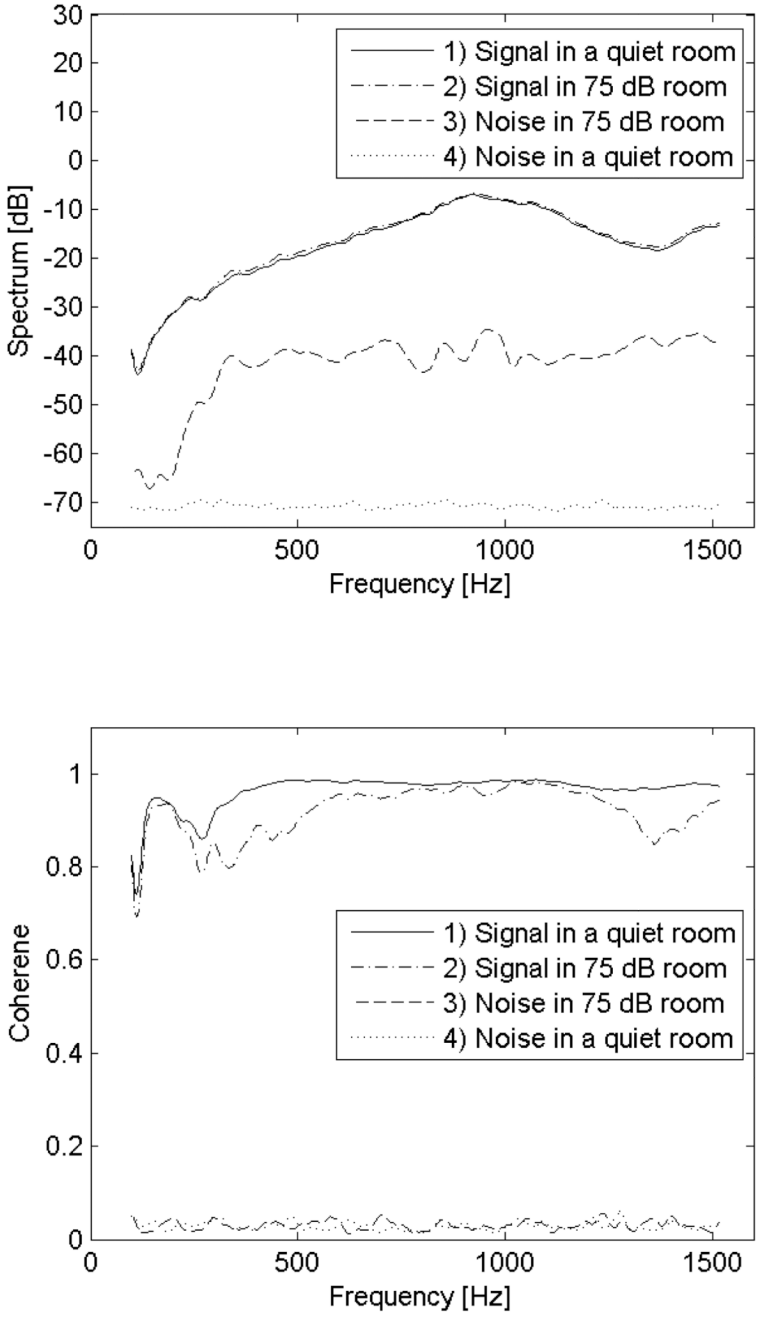

Fig. 8.

(a) The stethoscope output at different frequencies under four conditions: 1) in a quiet room while inputting a signal into the phantom (to measure contribution of the signal to the stethoscope output), 2) in a room with 75 dB noise while inputting a signal into the phantom, 3) in a room with 75 dB noise with no phantom input (to estimate room noise contribution to the sethoscope output), and 4) in a quiet room without a phantom input signal (to estimate the background noise)

(b) The coherence between the stethoscope output and phantom input at different frequencies under four conditions: 1) in a quiet room while inputting a signal into the phantom, 2) in a room with 75 dB noise while inputting a signal into the phantom, 3) in a

room with 75 dB noise with no phantom input, and 4) in a quiet room without a phantom input signal.